Macromolecules

pubs.acs.org/Macromolecules Article

Nanostructural Rearrangement of Lamellar Block Polymers Cured in the Vicinity of the Order−Disorder Transition

Nicholas Hampu and Marc A. Hillmyer*

Cite This: *Macromolecules* 2020, 53, 7691−7704 Read Online

ACCESS | Metrics & More | Article Recommendations | Supporting Information

ABSTRACT: The application of large amplitude oscillatory shear (LAOS) to block polymers near their order−disorder transition temperature (T_{ODT}) has previously been shown to induce morphological transitions and to promote domain alignment. To kinetically trap these transient shear-induced morphologies, we have utilized reactive poly(styrene-*stat*-glycidyl methacrylate)-*block*-polylactide diblock terpolymers that adopt lamellar morphologies in the quiescent state with thermally accessbile T_{ODT}'s and can readily be cross-linked near the T_{ODT} under LAOS. By maintaining a constant curing temperature in the disordered state while varying the strain amplitude, we observed a shear-induced transition from an isotropic fluctuating disordered morphology at low strain amplitude to an aligned parallel−transverse kinked lamellar morphology at high strain amplitude. Additionally, we investigated the effect that cross-linking temperature (distance from the T_{ODT}) at a constant strain amplitude had on the occurrence of shear-induced ordering. The large amplitude of composition fluctuations near the T_{ODT} was critical for the transition from a disordered to an ordered morphology under LAOS. Conversely, cross-linking temperatures *far* above T_{ODT} revealed the lack of a shear-induced disorder−order transition, possibly because of smaller amplitude fluctuations and/or rapid curing kinetics. These results suggest that careful selection of the strain amplitude and curing temperature during the cross-linking of lamellar block polymers under LAOS may enable the domain anisotropy and continuity to be precisely tailored for a targeted application.

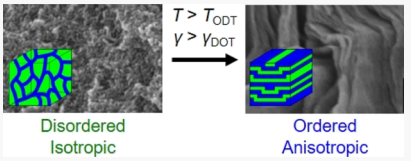

INTRODUCTION

Harnessing the self-assembly of materials is crucial for advancing numerous technologies, including energy storage and conversion,[1] water filtration,[2] and drug delivery.[3] Block polymers are particularly attractive for this purpose, as they can be designed to rationally target uniform and periodic patterns of tunable size and symmetry dictated by the molar mass, chemistry, and relative composition of the blocks.[4−6] Although strong enthalpic repulsions between the chemically dissimilar blocks drive these materials to microphase separation into ordered nanostructures at low temperatures and/or high degrees of polymerization (N), entropic factors associated with unfavorable chain stretching disrupt the long-range spatial correlations of the ordered state as the system is heated. Eventually, this results in an order to disorder transition (ODT) above T_{ODT}.[7] However, short-range microphase separation persists even above T_{ODT} because of composition fluctuations.[8−10]

Continued work is needed to precisely control the orientation and long-range spatial correlations of these self-assembled domains. The next-generation technologies generally rely upon either anisotropic lamellae or cylinders, which often require challenging processing methods to precisely orient their domains, or isotropic network structures (gyroid), which are difficult to access synthetically. Consequently, significant effort has been invested into manipulating the orientation of anisotropic domains through the application of solvent vapor annealing[11] and/or magnetic,[12] electric,[13] or shear fields.[14] Shear alignment techniques are particularly appealing as they facilitate uniform orientation of large sample volumes under relatively mild conditions.[15] The successful alignment of ordered lamellar and cylindrical morphologies under shear has been extensively documented in the literature.[14,16−19] However, there has been less work investigating the effect of shear fields on the domain structure of the disordered state.[16,20−22] Recently, our group has been exploring microphase separation above T_{ODT}, resulting from composition fluctuations.[23−26] This fluctuating disordered morphology was shown to exhibit a co-continuous nanostructure with potential practical utility in water filtration,[24] yet the high tortuosity of the domains may impose an undesirable resistance to transport for other applications.[27]

Therefore, we speculated that the application of large amplitude oscillatory shear (LAOS) during the in situ cross-linking of a lamellar-forming poly(styrene-*stat*-glycidyl methacrylate)-*block*-polylactide, P(S-*s*-GMA)-*b*-PLA, diblock polymer near the T_{ODT} can orient the nanostructured domains while still maintaining their highly desirable continuity. This study was motivated by the classic work of Koppi et al., which demonstrated that the application of LAOS above the T_{ODT}

Received: June 17, 2020
Revised: August 14, 2020
Published: September 3, 2020

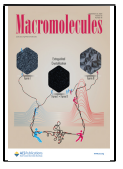

https://dx.doi.org/10.1021/acs.macromol.0c01424
Macromolecules 2020, 53, 7691−7704

can drive a disordered block polymer melt to transiently order into aligned lamellar or cylindrical domains because of a symmetry-breaking field that anisotropically suppresses composition fluctuations and effectively increases the T_{ODT}.[16,17,28] Although the expected disordered state was recovered following the cessation of shear for those uncross-linked systems, we believe that cross-linking P(S-*s*-GMA)-*b*-PLA above T_{ODT} under LAOS will kinetically trap this transient anisotropic morphology and allow for possible applications of this state.[16,24] Subsequent chemical etching of the PLA domains is expected to generate porous materials with tunable pore topologies and tortuosities that can potentially be tailored for targeted applications.

In this work, we examined the effect of strain amplitude at a constant cross-linking temperature above T_{ODT} for a P(S-*s*-GMA)-*b*-PLA diblock terpolymer containing the thermal acid generator benzyl triphenylphosphonium hexafluoroantimonate (BTPH).[24] Furthermore, we investigated the effect that the cross-linking temperature has on the orientation of these domains at a constant strain amplitude. To decouple the relative contributions of cross-linking and shearing on the observed morphologies, experiments were also performed on samples that were first cross-linked at low strain amplitude before applying LAOS after gelation. Through a combination of small-angle X-ray scattering (SAXS), scanning electron microscopy (SEM), and nitrogen sorption analysis, we revealed crucial processing-structure−property relationships that facilitate the design of tailored nanostructures with morphologies and domain orientations appropriate for a given application.

RESULTS AND DISCUSSION

Effect of Strain Amplitude on Domain Orientation above T_{ODT}. A readily cross-linkable P(S-*s*-GMA)-*b*-PLA diblock with a thermally accessible T_{ODT} was synthesized using a previously reported procedure (Figures S1−S3).[23,24] The diblock terpolymer examined in this section was comprised a 18 kg mol^{-1} PLA block and a 14 kg mol^{-1} P(S-*s*-GMA) block with a molar fraction of GMA (XGMA) of 0.29, which will be referred to as P(S-*s*-GMA)-14-PLA-18-XGMA-29. Variable temperature SAXS confirmed the targeted lamellar morphology with a periodicity of 25.8 nm and a T_{ODT} between 150 and 170 °C (Figures 1 and S4). Dynamic mechanical analysis (DMA) demonstrated a discontinuity in the temperature dependence of the storage modulus, G', around 160 °C, indicative of the T_{ODT} and in agreement with the results from SAXS (Figure 1).

After identifying the T_{ODT} for P(S-*s*-GMA)-14-PLA-18-XGMA-29, the thermal acid generator BTPH was selected as an appropriate cross-linking agent for the cationic polymerization of the pendant epoxide moieties of GMA.[24] Blends of P(S-*s*-GMA)-14-PLA-18-XGMA-29 containing 0.3 wt % BTPH were prepared by codissolution, solvent casting, and annealing overnight at 100 °C (gel time > 10 days) under reduced pressure prior to loading the samples into a rheometer. The samples were loaded in a parallel plate rheometer at 130 °C where the cross-linking kinetics were slow[24] (gel time > 1 day) and were then rapidly heated after several minutes to 168 °C (T_{ODT} + 8 °C). Upon reaching a steady-state temperature, oscillatory shear was applied. The gel time for P(S-*s*-GMA)-*b*-PLA + 0.3 wt % BTPH was previously found to be approximately 30 min at 170 °C, which is significantly longer than the approximately 1 min needed to reach a steady-state temperature at 168 °C. This ensures that oscillatory shear was applied to these samples prior to gelation,

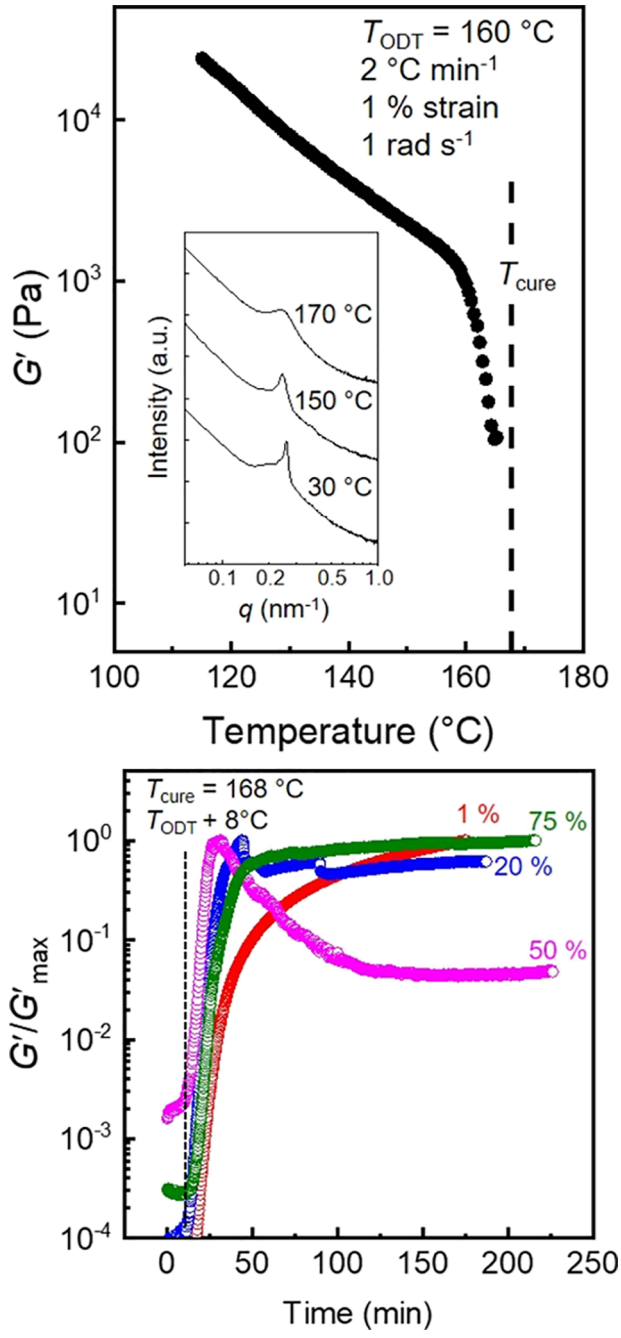

Figure 1. Dynamic temperature sweep for P(S-*s*-GMA)-14-PLA-18-XGMA-29 acquired at a strain amplitude of 1%, a frequency of 1 rad s^{-1}, and a heating rate of 2 °C min^{-1} (top). The precipitous drop in G' around 160 °C indicates the T_{ODT}, and the dashed line corresponds to the curing temperature used in subsequent experiments. Variable temperature SAXS patterns are in the inset and show a T_{ODT} between 150 and 170 °C, as indicated by significant peak broadening. Isothermal time sweeps obtained for P(S-*s*-GMA)-14-PLA-18-XGMA-29 + 0.3 wt % BTPH cured at 168 °C (bottom). Samples were cured under strain amplitudes of 1 (red circle, open), 20 (blue circle, open), 50 (pink circle, open), and 75% (green circle, open). To account for shear thinning, $G'(t)$ was normalized by the maximum G' observed for each sample. The gel time is indicated by a dashed black line. P(S-*s*-GMA)-14-PLA-18-XGMA-29 was in the nonlinear viscoelastic regime for strain amplitudes of 20% and above.

https://dx.doi.org/10.1021/acs.macromol.0c01424
Macromolecules 2020, 53, 7691−7704

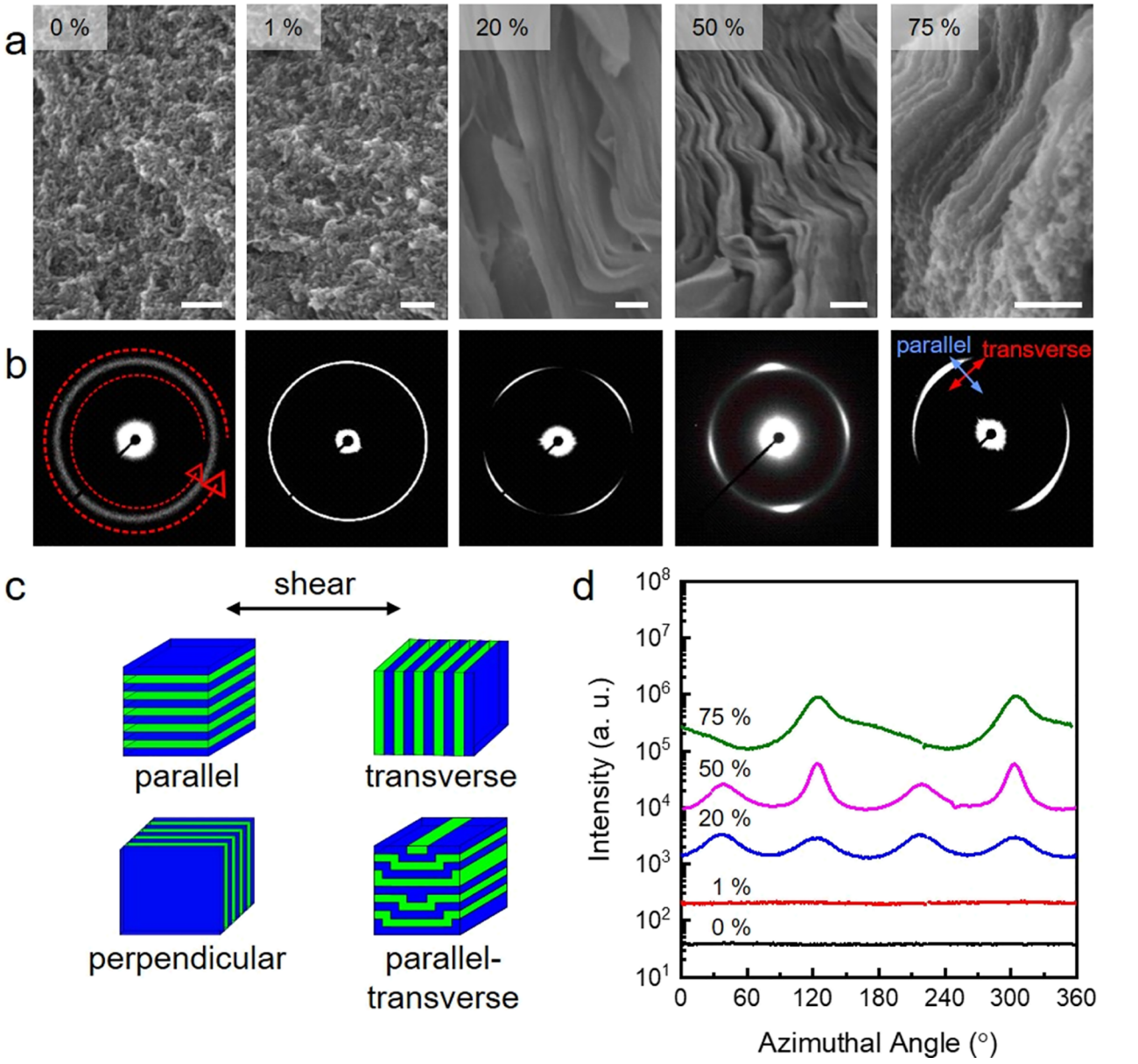

Figure 2. SEM images for P(S-*s*-GMA)-14-PLA-18-XGMA-29 + 0.3 wt % BTPH cured at 168 °C (T_{ODT} + 8 °C) under strain amplitudes of 0, 1, 20, 50, and 75% following PLA removal (a). Scale bars correspond to 200 nm for each SEM image. All SEM samples were coated with approximately 2 nm of Ir and imaged at 3.0 kV. 2D SAXS patterns of the parallel−transverse (tangential) plane for the same samples prior to PLA removal are presented in (b). The path corresponding to the azimuthal integration is indicated by the red dashed arrows, where the arrow tail represents an azimuthal angle of 0°, and the arrow head approaches 360°. The directions corresponding to morphological features that are parallel and transverse to the shearing direction for the chosen sample configuration are indicated on the final pattern. These directions apply to all samples shown in (b) slight variations in the azimuthal angles were a result of sample loading into the SAXS geometry. Illustrations of parallel, perpendicular, transverse, and parallel−transverse kinked lamellar orientations with respect to the shearing direction are provided in (c). Integrated intensities of the 2D SAXS patterns as a functional of azimuthal angle along the principal scattering vector for each strain amplitude are presented in (d).

but certainly, some cross-linking has begun after reaching 168 °C.[24] Five different strain amplitudes were investigated: 0, 1, 20, 50, and 75%. Isothermal time sweeps were acquired for each nonzero strain amplitude during the in situ cross-linking at 168 °C to monitor the evolution of G' over time (Figures 1 and S5).

Each rheological time sweep demonstrated a rapid increase in both G' and G'' at early time points, signaling the onset of the cross-linking reaction (Figures 1 and S5). The values of G' and G'' cross after approximately 17−20 min for all sample, indicating that the gel time was unaffected by strain amplitude (Figure S5). After gelation, G' initially continued to increase with time for all samples, eventually reaching a maximum or a plateau value. Generally, higher values of G'_{max} were observed at lower strain amplitudes, likely because of shear thinning behavior at high strain. In contrast, a sample of P(S-*s*-GMA)-14-PLA-18-XGMA-29 without BTPH displayed G'' values greater than G' values and no noticeable increase in G' and G'' over time, confirming that the observed behavior was a direct result of BTPH-catalyzed cross-linking (Figure S6). We note that P(S-*s*-GMA)-14-PLA-18-XGMA-29 was outside of the linear viscoelastic regime for the experimental strain

https://dx.doi.org/10.1021/acs.macromol.0c01424
Macromolecules 2020, 53, 7691−7704

amplitudes of about 20% and above (Figure S7), so we do not make quantitative comparisons across different strain amplitudes. However, a qualitative analysis of the time evolution of G' (and particularly of $G'(t)/G'_{max}$) for a given strain amplitude was still informative.

For the smallest measurable strain amplitude of 1%, the G' plateaued at long experimental times, consistent with the typical behavior of cross-linked materials. In contrast, the samples that were cured under LAOS at 20 and 50% strain displayed a gradual decrease in apparent G' after reaching an initial maximum. The extent of the decrease in G' was dependent upon the magnitude of the strain amplitude, with higher strain amplitudes generally corresponding to larger decreases in the storage modulus. Because the gel fraction of these samples all approached 1, we posit that the decrease in G' over time represented a change in the extent of domain orientation rather than a change in the degree of cross-linking or sample degradation. Similar behavior has been previously attributed to the parallel alignment of lamellae for uncross-linked block polymers subjected to LAOS in the vicinity of the T_{ODT}, where the introduction of slip planes lowered G'.[29,30] A factor of 15 decrease in G' was observed for a strain amplitude of 50%, which was significantly greater than the factor of 5 decrease that has been observed for uncross-linked systems.[30] Furthermore, no significant change in G' over time was observed for samples that did not contain BTPH sheared at 150 and 170 °C under 50% strain, consistent with the conclusion that the large reduction in the storage modulus was a consequence of the cross-linked nature of these samples (Figure S6). We expect that the cross-links introduced spatial and orientational correlations that drove the collective motion of the cured domains under LAOS and ultimately facilitated domain alignment.

Interestingly, no such decay in G' was observed over time for the sample cross-linked at the highest investigated strain amplitude of 75%. Although this result seems contradictory to the hypothesized rheological signature of domain orientation, one possible explanation for the observed results could be related to the complex interplay between the relative kinetics of curing and domain orientation. The sample sheared at 75% strain amplitude exhibited the lowest viscosity and highest driving force for domain alignment. Therefore, we believe that the domain orientation kinetics should be fastest at 75% strain amplitude. As a result, the lamellar domains may be highly oriented parallel to the shearing direction prior to the completion of the cross-linking reaction. This introduces a competing effect between an increasing G' from cross-linking and a decreasing G' from domain alignment, consistent with the observed slower initial increase of G' over time for 75% strain amplitude as compared to 50% strain amplitude. By the time the cross-linking reaction has reached complete conversion, the lamellae are already completely aligned parallel to the shearing direction, and no subsequent decay in G' is observed for 75% strain amplitude. The different viscoelastic properties observed at 75% strain amplitude as compared to 20 and 50% strain amplitude may reflect changes in the domain nanostructure with increasing strain, which we address below.

To more directly evaluate the effect of strain amplitude on the degree of domain anisotropy, SAXS and SEM were performed on each sample (Figures 2, S8 and S9). All SAXS patterns were obtained for samples prior to PLA removal to provide information regarding global domain orientation without introducing complications related to the mechanical stability of porous nanostructures. SAXS patterns were acquired ex situ by sectioning the cured samples along predetermined orientations with respect to the shearing direction. Samples were approximately 3 mm thick in the through-beam direction, and the X-ray beam was incident in the center of the sample with a diameter of 1 mm. The scattered intensity is presented in arbitrary units, and quantitative comparisons of intensity between different samples are not possible, but relative comparisons of scattered intensity for a given sample are informative. SEM was performed on the same samples after PLA removal to improve imaging contrast and to provide information related to the local nanostructure. For low strain amplitudes of 0 and 1%, a single isotropic ring with a scattered intensity independent of the azimuthal angle was observed by SAXS, consistent with unoriented and disordered domains. SEM images of these samples confirmed their disordered nature, as a reticulated morphology that resembled other fluctuating disordered samples was observed.[23,24]

However, the samples cross-linked under LAOS with strain amplitudes ≥20% displayed noticeable anisotropy in their 2D SAXS patterns. Strain amplitudes of 20 and 50% resulted in SAXS patterns comprising four spots oriented at 90° intervals in the parallel−transverse plane, suggestive of aligned domains (Figure 2b). No higher order scattering peaks were observed, likely because of the proximity of the curing and shearing temperature to the T_{ODT}. Near the T_{ODT}, the composition profile is sinusoidal, and the Fourier transform of a sinusoidal wave results in a delta function centered around q^*. Consequently, no higher order peaks are observed near the T_{ODT}, preventing the definitive assignment of the morphology by SAXS alone. Therefore, SEM images of these samples acquired postetching were used to reveal the local nanostructure. A sheet-like morphology that resembled lamellar ordering despite a cross-linking temperature that was above the T_{ODT} was observed for strain amplitudes of 20 and 50% (Figure 2a).[31] Consequently, we attributed the lamellar morphology and domain anisotropy of the 20 and 50% samples to a shear-induced disorder−order transition (DOT).[16,28] The application of LAOS anisotropically suppressed composition fluctuations and effectively raised the T_{ODT}, similar to observations by Koppi et al. for uncross-linked systems.[16,28] In contrast, a sample that did not contain BTPH and was sheared at 170 °C under a strain amplitude of 50% displayed an unoriented and disordered morphology by SEM after cooling to ambient temperature (Figure S10). We expect that this sample also experienced a shear-induced DOT, but the cooling rate was too slow to trap the transient ordered morphology upon the cessation of shear. Therefore, the shear-induced lamellar morphology first relaxed into an isotropic disordered state and was then kinetically trapped in this disordered state by vitrification before it could nucleate the thermodynamically favored ordered state below T_{ODT}. This demonstrates the critical role that the cross-linking reaction plays in kinetically trapping an otherwise transient shear-induced morphology.

Curiously, the four-spot pattern observed in the parallel−transverse plane suggested the presence of domains with the four-fold symmetry rather than the two-fold symmetry expected for a uniformly aligned lamellar morphology (see Figure 2c for illustrations of possible lamellar orientations with respect to the shearing direction). Additionally, SAXS patterns obtained in the parallel−perpendicular plane generally displayed anisotropic features along the parallel direction

https://dx.doi.org/10.1021/acs.macromol.0c01424
Macromolecules 2020, 53, 7691−7704

(and in some cases along the perpendicular direction), as shown in Figure S9. Based on these results, we surmised that the domains primarily adopted a parallel−transverse kinked lamellar morphology, where the predominantly parallel lamellae are folded in the transverse direction at tilt boundaries.[18,19,32,33] Although some of the SEM images appear to contain such kinked lamellae, the size-scale of the high-magnification SEM images only provides the local domain nanostructure, and definitive conclusions regarding the long-range domain orientation are limited to the SAXS analysis. Previous work[33] has demonstrated that a large mechanical contrast between domains under LAOS results in the formation of preferential slip planes in one domain. These slip planes cannot occur across the intermaterial dividing surface because of the connectivity between the blocks, so slip occurs within the lamellar domain with the lower modulus.[33] The intermolecular cross-links and significantly higher modulus of the P(S-*s*-GMA) domains resulted in a high mechanical contrast between the domains. This limited deformation to the softer PLA domains along preferential slip planes. To relax the high shear stresses present under LAOS, the parallel lamellae likely buckle along these slip planes to form transversely (and also in some cases perpendicularly) oriented hinges.[19,32,33] These conclusions are generally consistent with previous work on the orientation of uncross-linked lamellar diblocks under LAOS.[19,32,33]

For an even higher strain amplitude of 75%, SAXS patterns displayed only two spots parallel to the shear direction that was oriented at 180° intervals and displayed small shoulders. This suggested that the lamellae were primarily oriented parallel to the shear direction without the kink bands observed at lower strain amplitude. The SEM image for this sample exhibited some regions consistent with lamellar ordering; however, there were also regions that resembled the disordered state. We hypothesized that these disordered regions reflected the fracturing of the lamellar domains at the transverse hinges because of the high normal stresses present at large strain amplitude.

The ability to produce porous materials from these shear-oriented materials by removing the PLA domains provided a valuable tool to quantitively probe the continuity of their domains using Brunauer−Emmett−Teller (BET) analysis (Figure 3).[24,34] All samples exhibited quantitative PLA removal by gravimetric analysis, suggesting that the PLA domains were accessible to the etching solution, consistent with previous results for ordered lamellar and fluctuating disordered morphologies.[24] The unsheared sample (0% strain) displayed a N_2 sorption isotherm characteristic of a mesoporous material and consistent with the bicontinuous morphology of the fluctuating disordered state.[24,34] These results corresponded well with the isotropic and disordered morphology revealed by SAXS and SEM. The samples cured under 20 and 50% strain also exhibited relatively high levels of mesoporosity, albeit slightly lower than for the unsheared sample. The measurable porosity for these samples despite their lamellar ordering was surprising, as we have previously reported that unaligned and etched lamellar morphologies were essentially nonporous because of the collapse of the mechanically unstable free-standing sheets.[24,25,31,35] We believe that the stable pores observed in this work may be a consequence of the parallel−transverse kinked lamellae, where the hinge regions orthogonal to the parallel lamellae reinforce against pore collapse following PLA removal. Furthermore, the comparably high porosities for

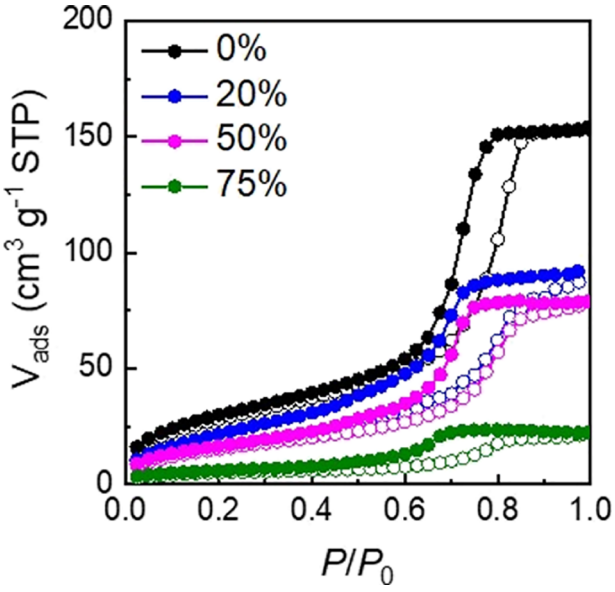

Figure 3. Nitrogen sorption isotherms for P(S-*s*-GMA)-14-PLA-18-XGMA-29 + 0.3 wt % BTPH cured at 168 °C (T_{ODT} + 8 °C) under strain amplitudes of 0, 1, 20, 50, and 75% following PLA removal.

the disordered morphology obtained in the unsheared case and for the oriented and kinked lamellar morphology obtained under 20 and 50% strain suggest that the domain continuity of the fluctuating disordered state and the ordered lamellar state is quite similar.[8] From a practical perspective, this strategy could be a useful approach to control the tortuosity of bicontinuous domains and thus remove physical barriers that hinder mass transport without compromising domain continuity. An even higher strain amplitude of 75% resulted in a significantly lower porosity, likely because of fracturing of the lamellar domains at these high shear stresses as observed in SEM and SAXS. Consequently, the continuity of the domains was interrupted. These results demonstrate the utility of LAOS for precisely controlling the morphology and domain orientation near the T_{ODT}, enabling the engineering of targeted nanostructures.

Temperature Dependence of Domain Orientation under LAOS. In addition to strain amplitude, we expected that the cross-linking temperature would also significantly influence the extent of domain alignment under LAOS. To explore this, we selected the diblock polymer P(S-*s*-GMA)-17-PLA-23-XGMA-27 with a T_{ODT} of approximately 170 °C by DMA (Figure 4) and a lamellar morphology with a domain spacing of 28.9 nm by SAXS (Figure S11). Three different cross-linking temperatures (155, 175, and 190 °C) were investigated at two different strain amplitudes (0 or 50%) to study the effect that LAOS had on domain alignment during the in situ cross-linking in the ordered state (T_{ODT} − 15 °C = 155 °C, t_{gel} = 3.5 h), the strongly fluctuating disordered state (T_{ODT} + 5 °C = 175 °C, t_{gel} = 0.5 h), and the weakly fluctuating disordered state (T_{ODT} + 20 °C = 190 °C, t_{gel} = 6 min).

All samples were loaded into a parallel plate rheometer at 130 °C and rapidly heated to the targeted cross-linking temperature, as described previously. Upon reaching the desired temperature, isothermal time sweeps were performed under LAOS with a strain amplitude of 50% (Figures 4 and S12). Qualitatively, similar rheological behavior to the samples

https://dx.doi.org/10.1021/acs.macromol.0c01424
Macromolecules 2020, 53, 7691−7704

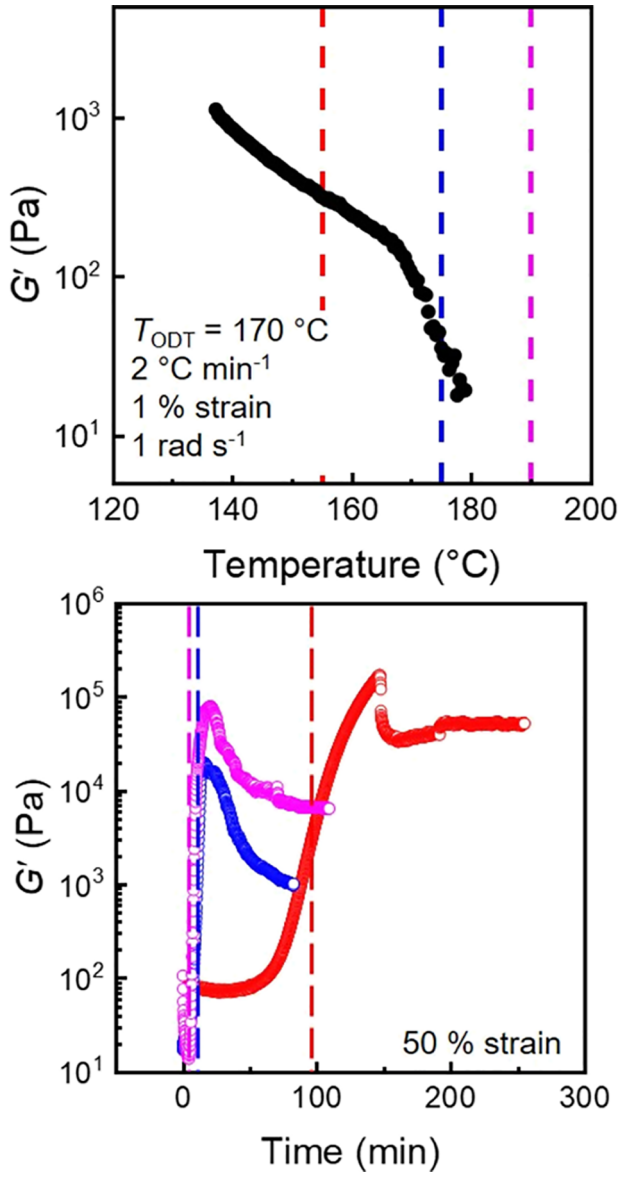

Figure 4. Dynamic temperature sweep for P(S-*s*-GMA)-17-PLA-23-XGMA-27 acquired at a strain amplitude of 1%, a frequency of 1 rad s^{-1}, and a heating rate of 2 °C min^{-1} (top). The precipitous drop in G' around 170 °C indicates the T_{ODT}, and the dashed lines correspond to the curing temperatures used in subsequent experiments. Isothermal time sweeps for P(S-*s*-GMA)-17-PLA-23-XGMA-27 + 0.3 wt % BTPH for samples cured at 155 (red circle, open), 175 (blue circle, open), and 190 (pink circle, open) °C under a strain amplitude of 50% (bottom). Gel times for each curing temperature are indicated by the dashed lines.

cured under variable strain amplitude was observed. The gel time was a function of temperature and ranged from 8 min at 190 °C to 95 min at 155 °C. After the apparent G' reached its initial maximum at intermediate time points, it decayed over time because of domain alignment.[29,30] The extent of this decay was highest for the cross-linking temperatures closest to the T_{ODT}, where composition fluctuations have the highest amplitude in the unsheared state.[8,36] Qualitatively, similar trends were observed for P(S-*s*-GMA)-17-PLA-23-XGMA-27 + 0.3 wt % BTPH cured under 50% strain at 165, 180, and 210 °C (Figure S12).

Following curing, SAXS and SEM were used to analyze the morphology and domain anisotropy for the sheared and the unsheared samples (Figures 5 and S13). Again all SAXS patterns were obtained for unetched and nonporous materials, and all SEM images were acquired for etched and porous samples. For the sample cured at 155 °C (T_{ODT} − 15 °C) without shear, a sharp and isotropic ring was observed in the SAXS pattern, characteristic of an ordered morphology. This morphology was found to be lamellae by the SEM image obtained after etching. Although some evidence of kinking may be found in the SEM image, SEM only probes the local nanostructure while SAXS suggests that the lamellae are unoriented across large length scales. The sample cured at the same temperature under LAOS exhibited a noticeably different SAXS pattern comprising four spots oriented at 90° intervals along with a layered morphology by SEM, consistent with the parallel−transverse kinked lamellae described previously.[18,32] Therefore, the application of LAOS during the in situ curing of a diblock polymer in the ordered state aligned the lamellae without inducing a morphological transition.

For the sample cured at 175 °C (T_{ODT} + 5 °C), the SAXS pattern for the unsheared sample displayed a diffuse and isotropic ring indicative of a disordered morphology and consistent with the fluctuating disordered morphology observed by SEM. Cross-linking the same polymer at the same temperature under LAOS resulted in a strikingly different morphology. The SAXS pattern revealed four spots suggesting domain anisotropy, and SEM showed a layered morphology that resembled the lamellar state despite being nominally cured above T_{ODT}. These results corresponded well with those discussed previously for varying strain amplitude at a constant curing temperature slightly above T_{ODT}, and they demonstrate the generality of the shear-induced DOT for different block polymers. In contrast, the application of 1% strain during the in situ cross-linking at 175 °C resulted in an less anisotropic SAXS pattern, and a disordered morphology by SEM (Figure S14), demonstrating that large strain amplitudes are critical for generating the symmetry breaking field necessary for inducing the morphological transformation from a disordered and bicontinuous state to an aligned lamellar state.[16,21,28]

Finally, the samples cured well above the T_{ODT} at 190 °C (T_{ODT} + 20 °C) exhibited negligible differences between the samples cured under 0 and 50% strain by SAXS and SEM. Both samples had disordered and isotropic morphologies consistent with those that have previously been reported for block polymers cross-linked above T_{ODT}. These results may suggest that the existence of large amplitude composition fluctuations near the T_{ODT} played a key role in the morphological transition that occurred under LAOS. The observance of such a transition for cross-linking temperatures slightly above T_{ODT} (175 and 180 °C, T_{ODT} + 5 and 10 °C) and the absence of the transition for cross-linking temperatures *far* above T_{ODT} (190 and 210 °C, T_{ODT} + 20 and 40 °C) support this conclusion (Figure S15). Theory has predicted that LAOS anisotropically suppresses composition fluctuations, thereby stabilizing the ordered state and effectively raising T_{ODT} toward the mean-field limit.[28] For cross-linking temperatures that were slightly higher than T_{ODT} (175 and 180 °C), the suppression of large amplitude fluctuations may have effectively increased the T_{ODT} above the curing temperature and induced ordering.[16] In contrast, for higher temperatures (190 and 210 °C), the elevated T_{ODT} under LAOS was possibly still below the curing temperature, and the sample

https://dx.doi.org/10.1021/acs.macromol.0c01424
Macromolecules 2020, 53, 7691−7704

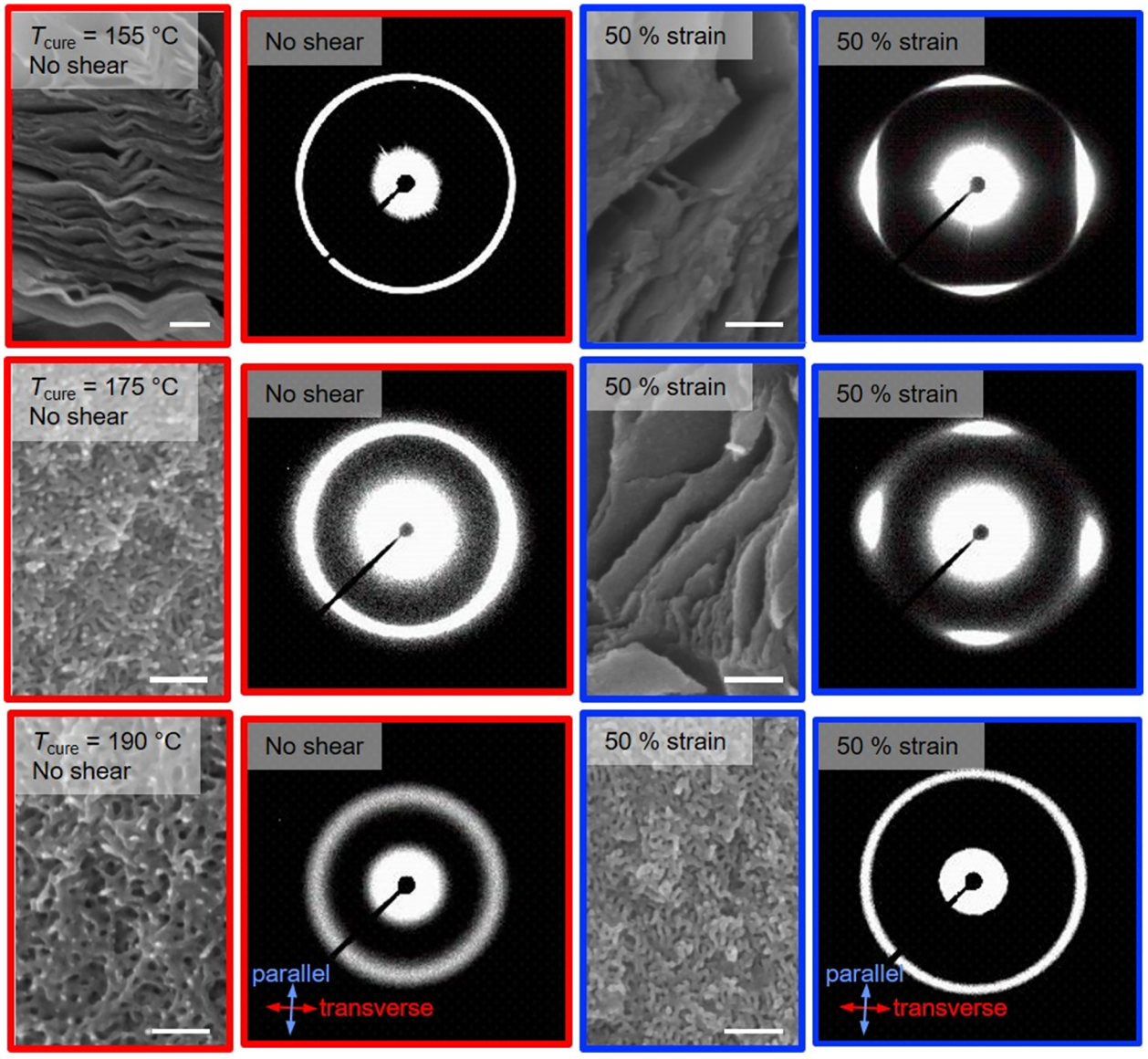

Figure 5. SEM images and 2D SAXS patterns of P(S-*s*-GMA)-17-PLA-23-XGMA-27 + 0.3 wt % BTPH cured at 155 °C (T_{ODT} − 15 °C, top row), 175 °C (T_{ODT} + 5 °C, middle row), and 190 °C (T_{ODT} + 20 °C, bottom row). Samples were cured in the absence of shear (red borders, first and second columns) and under LAOS with a strain amplitude of 50% (blue borders, third and fourth columns). SAXS patterns were obtained prior to PLA removal, and SEM images were obtained following PLA removal. The scale bar corresponds to 200 nm for all SEM images. All SEM samples were coated with approximately 2 nm of Ir and imaged at 3.0 kV. The directions parallel and transverse to the shearing direction for all samples are indicated by the arrows in the bottom row of SAXS patterns.

remained disordered. A visual depiction of the evolution of the hypothesized domain structure as a function of curing temperature and strain amplitude is presented in Figure 6.

After establishing that LAOS could induce domain orientation in these cross-linked samples, N_2 sorption analysis was performed on P(S-*s*-GMA)-17-PLA-23-XGMA-27 samples cured in both the absence of shear and under LAOS to establish correlations between the morphology, domain orientation, and domain continuity (Figures 7 and S16). Quantitative PLA removal was again observed for all samples, suggesting that the PLA domains were accessible to the etching solution. Samples cured below the nominal T_{ODT} exhibited negligible porosity for both the unsheared and sheared samples. Although these results may appear to be in conflict with the complete removal of PLA confirmed by gravimetric analysis, they are consistent with previous work that reported a lack of measurable porosity for diblocks cross-linked in the ordered lamellar state because of the collapse of the mechanically unstable lamellae.[24,25,31,35]

A noticeable increase in the BET surface area was observed for the unsheared sample cross-linked at 175 °C (T_{ODT} + 5 °C), as the bicontinuous nature of the fluctuating disordered state enhanced the connectivity of the pore network, as we have established previously.[24,25,35] This conclusion was supported by the morphological picture obtained from SAXS and SEM. Interestingly, the sample cured under LAOS (50% strain) at 175 °C displayed an even higher porosity than the unsheared sample despite exhibiting a lamellar morphology by SEM and SAXS. This result was inconsistent with previous reports that directly correlated the disordered morphology to the high degree of pore continuity.[24] Furthermore, the samples cured under LAOS at T_{ODT} − 5 °C displayed the expected lack

https://dx.doi.org/10.1021/acs.macromol.0c01424
Macromolecules 2020, 53, 7691−7704

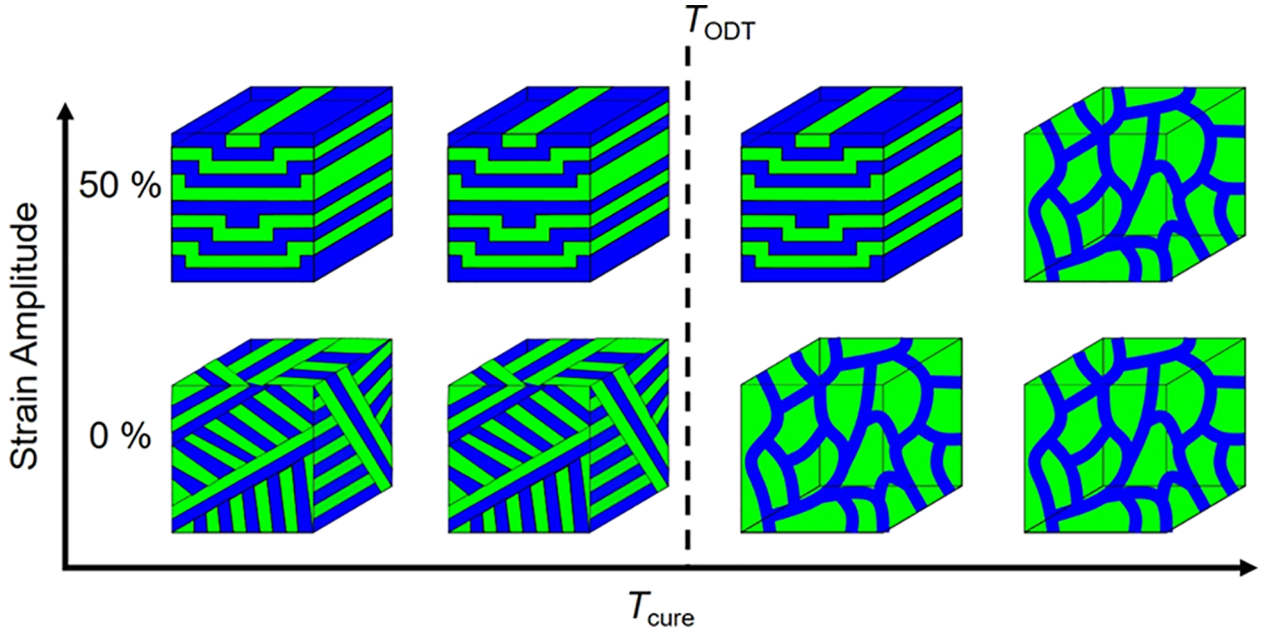

Figure 6. Schematic depicting the hypothesized morphological evolution as a function of curing temperature and strain amplitude near the T_{ODT}. The *x*-axis indicates curing temperature relative to the T_{ODT}, and the *y*-axis indicates strain amplitude.

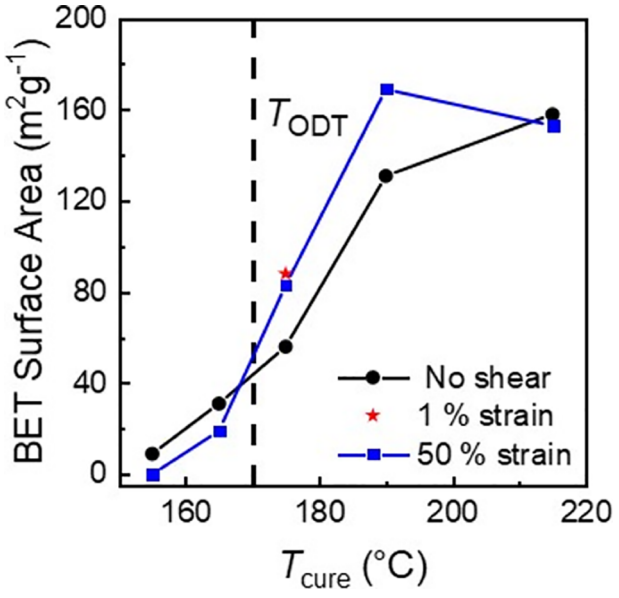

Figure 7. BET surface areas for P(S-*s*-GMA)-17-PLA-23-XGMA-27 + 0.3 wt % BTPH samples cured under various strain amplitudes are presented as a function of curing temperature. Samples were cured with strain amplitudes of 0% (circle solid), 1% (red star solid), and 50% (blue box solid). The T_{ODT} of the uncured block polymer precursor is denoted by a dashed line. The typical error in the calculation of the BET surface area is in the range of 5−10 m^2 g^{-1}.

of porosity despite exhibiting a morphology that was similar to the sample cured at T_{ODT} + 5 °C, suggesting that shear alignment alone did not enhance the porosity. This interesting discrepancy may be related to the shear-induced DOT observed for the sample subjected to LAOS at T_{ODT} + 5 °C. Theory has suggested that the ODT is a topological transition dictated by a change in interfacial curvature rather than domain composition.[8,36,37] Therefore, LAOS may have effectively reorganized the interfaces of the fluctuating disordered state into a kinked lamellar morphology with a degree of domain continuity and mechanical stability similar to the disordered state. This observation merits further investigation. Finally, similarly high BET surface areas were measured for both the unsheared and shear aligned samples cross-linked at temperatures well above T_{ODT}, consistent with their relatively similar morphologies observed by SAXS and SEM. As discussed previously, this behavior may be related to the lack of coupling between LAOS and the smaller amplitude of composition fluctuations at these higher temperatures.

However, the lack of domain orientation at high curing temperatures could instead be a consequence of the fast cross-linking kinetics at 190 and 210 °C. The gel times for P(S-*s*-GMA)-*b*-PLA + 0.3 wt % BTPH are 6 and 1 min at 190 and 210 °C, respectively.[24] Gelation thus occurs on a similar timescale as the approximately 1 min required for the rheometer to establish a steady state at the curing temperature. Therefore, it is likely that the samples cured at the highest temperatures (and *far* above T_{ODT}) were already highly cross-linked prior to the onset of LAOS, although the observance of a crossover between G' and G'' suggests that complete gelation had yet to occur before shearing. If the degree of cross-linking is too high prior to the onset of LAOS, the domains could be kinetically trapped in an isotropic and disordered morphology and unable to readily reorganize into aligned domains under shear. Furthermore, the relative kinetics of the cross-linking reaction compared to the kinetics of domain orientation can potentially alter the microstructure of the cross-linked domain (e.g., the cross-link density and mesh size), which could in turn influence the nanostructured morphology.

To test this hypothesis, a sample of P(S-*s*-GMA)-17-PLA-23-XGMA-27 + 0.3 wt % BTPH was first cured at 180 °C under a very low strain amplitude of 0.1%, as monitored by an isothermal time sweep in DMA (Figure S17). After completion of the cross-linking reaction, a large strain amplitude of 50% was immediately applied while maintaining the curing temperature. A large and instantaneous drop in G' was observed after increasing the strain amplitude to 50% (Figure S17). After this initial drop, G' remained relatively constant

https://dx.doi.org/10.1021/acs.macromol.0c01424
Macromolecules 2020, 53, 7691−7704

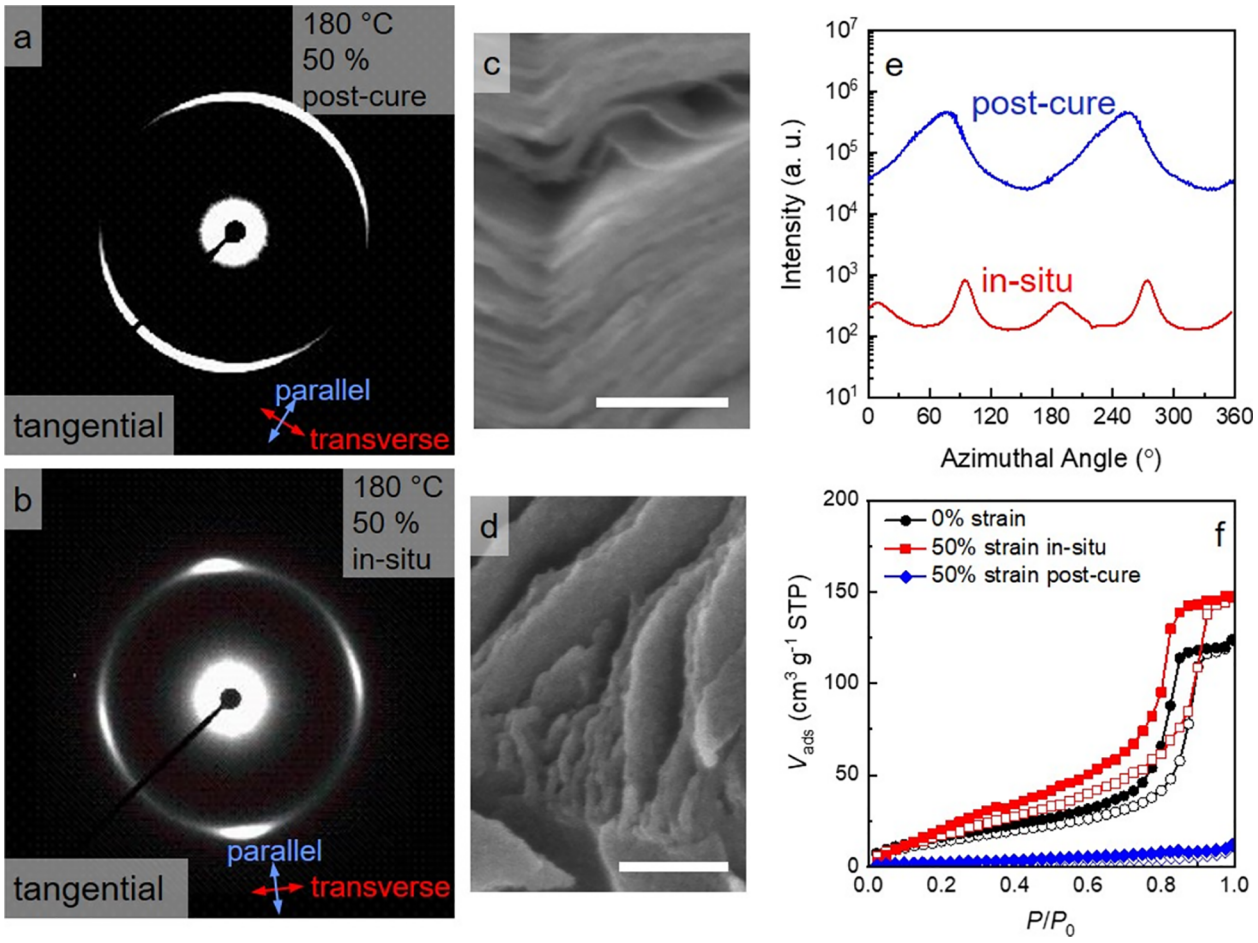

Figure 8. 2D SAXS patterns of the parallel−transverse (tangential) plane prior to PLA removal (a,b) and SEM after PLA removal (c,d) are presented for P(S-*s*-GMA)-17-PLA-23-XGMA-27 + 0.3 wt % BTPH cured at 180 °C. One sample (postcure) was first cured under a strain amplitude of 0.1% and then sheared under a strain amplitude of 50% postgelation (a,c). The other sample (in situ) was cured under a strain amplitude of 50% (b,d). The directions that correspond to morphological features that are parallel and transverse to the shearing direction for each scattering pattern are inset in (a,b). Integrated intensities of the 2D SAXS patterns as a functional of azimuthal angle along the principal scattering vector (e) are presented for patterns shown in (a,b). Nitrogen sorption isotherms are presented for the same samples after PLA removal in (f).

over the timescale of the experiment in contrast to the large decay previously observed for the sample that was cross-linked under LAOS at this same temperature (Figure S14). The sample was cooled to ambient temperature at approximately 20 °C min^{-1} and then removed from the rheometer and analyzed using SAXS (Figures 8 and S18).

In contrast to the four-spot scattering pattern observed for the sample cross-linked under LAOS, a two-spot pattern consistent with domains oriented parallel to the shear direction was observed for the sample sheared post-curing (Figure 8a,b). SEM of this sample after PLA removal revealed a lamellar morphology that appeared to be qualitatively similar to the sample cured under LAOS, again suggesting a shear-induced DOT (Figure 8c,d). These results suggest that even samples that were cross-linked prior to the application of LAOS had sufficient chain mobility to reorganize into oriented domains upon shearing. However, the change from a SAXS pattern consistent with parallel−transverse kinked lamellae for the sample cured under LAOS to a SAXS pattern consistent with purely parallel lamellae for the sample subjected to LAOS postcuring is intriguing. These differences may suggest that the parallel−transverse kink bands may arise because of the complex interplay between stress relaxation and network formation during simultaneous shearing and curing. As mentioned previously, the occurrence of simultaneous cross-linking and domain alignment can alter the local chain connectivity in the cross-linked domains and thus the overall morphology as compared to a sample that was first cross-linked and subsequently shear aligned. Such behavior may also be related to the previously discussed lamellar fracture observed for P(S-*s*-GMA)-14-PLA-18-XGMA-29 + 0.3 wt % cured under 75% strain, where the precured domains lack the requisite mobility to relax these high shear stresses by forming kink bands. However, further investigation is required to make any definitive conclusions on either point. Additionally, the porosity of the sample subjected to LAOS post-curing was significantly lower than for the samples that were cured at the same temperature in the absence of shear and under LAOS. The high levels of parallel orientation of these lamellae were likely mechanically unstable after PLA removal and resulted in pore collapse, as has been previously observed for unoriented lamellae.[24,31] In contrast, the parallel−transverse kinked lamellae appear to have a higher mechanical stability, and this resulted in a similar porosity to the unsheared and disordered sample.

Similar experiments were performed P(S-*s*-GMA)-14-PLA-18-XGMA-29 + 0.3 wt % BTPH (Figure S19). A sample was first cured at 170 °C (T_{ODT} + 10 °C) with a strain amplitude of

https://dx.doi.org/10.1021/acs.macromol.0c01424
Macromolecules 2020, 53, 7691−7704

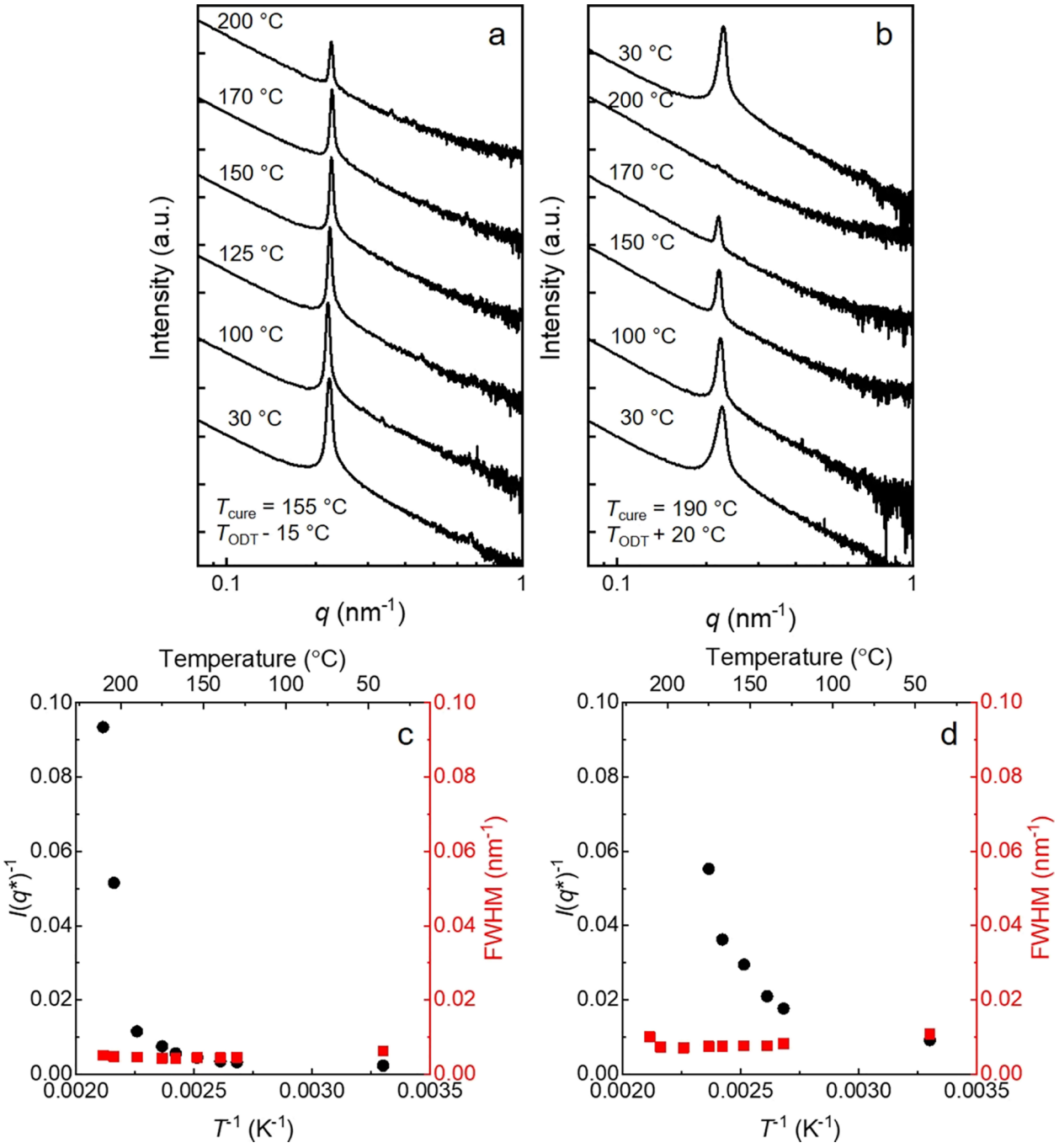

Figure 9. Variable-temperature SAXS patterns for P(S-*s*-GMA)-17-PLA-23-XGMA-27 + 0.3 wt % BTPH cured in the ordered state at 155 °C (T_{ODT} − 15 °C, a) and in the disordered state at 190 °C (T_{ODT} + 20 °C, b). The samples were cured at the specified temperatures and then annealed overnight at 100 °C under reduced pressure prior to data acquisition. Samples were equilibrated for 2 min at each experimental temperature. The inverse intensity of the principal scattering peak, $I(q^*)^{-1}$ and the full-width at half maximum (FWHM) of the principal scattering peak are plotted as a function of inverse temperature for T_{cure} = 155 (c) and 190 °C (d).

0.1%. The strain amplitude was then immediately increased to 50%, following the completion of the cross-linking reaction. Curiously, only a very slight degree of domain orientation parallel to the shear direction was observed in SAXS in contrast to P(S-*s*-GMA)-17-PLA-23-XGMA-27, suggesting that the domains were mostly unoriented (Figures S20 and S21). However, SEM images of this sample after PLA removal displayed a lamellar morphology, indicating that a shear-induced DOT had occurred despite the lack of domain alignment (Figure S20). These results reflect that the symmetry breaking shear field was sufficient to suppress composition fluctuations and induce ordering but it was insufficient to orient the domains. Because of its lower molar mass and higher XGMA, the cross-link density of P(S-*s*-GMA)-14-PLA-18-XGMA-29 was expected to be higher than of P(S-*s*-GMA)-17-PLA-23-XGMA-27. The chain mobility of this more heavily cross-linked polymer is expected to be restricted, hindering domain reorientation under LAOS.[22] This point merits further investigation, and a potential hypothesis for this

https://dx.doi.org/10.1021/acs.macromol.0c01424
Macromolecules 2020, 53, 7691−7704

proposed mechanism will be discussed in more detail in the following section.

Effect of Cross-Linking on the ODT. To better understand the mechanisms behind domain reorganization in the cross-linked state under LAOS, P(S-*s*-GMA)-17-PLA-23-XGMA-27 + 0.3 wt % BTPH was cross-linked and subsequently analyzed using variable-temperature SAXS. Two different cross-linking temperatures were selected: 155 °C (T_{ODT} − 15 °C) and 190 °C (T_{ODT} + 20 °C). After cross-linking, the samples were ambiently cooled to room temperature and then annealed overnight at 100 °C under reduced pressure to prevent decomposition. The temperature dependence of the cross-linked morphology was then investigated using SAXS (Figure 9).

For the sample cured in the ordered state at 155 °C, a sharp principal scattering peak was observed at 30 °C, indicative of an ordered morphology and consistent with cross-linking below T_{ODT}. As the sample that was heated to 200 °C, a noticeable decrease in the intensity of the principal scattering peak was observed. Indeed, a rapid increase in the inverse intensity of the principal scattering peak, $I(q^*)^{-1}$, was observed beginning around 170 °C. Such behavior is generally consistent with an ODT,[9] and the onset of this behavior was consistent with the T_{ODT} of the uncross-linked sample. This appears to suggest that the ODT is still accessible for this sample despite being cross-linked, which is consistent with previous observations for moderately cross-linked block polymers.[38,39] However, it is interesting to note that the FWHM for the principal scattering peak remained nearly constant across the entire temperature range. This observation is inconsistent with the generally observed peak broadening (as indicated by a large increase in FWHM) as a sample is heated through the T_{ODT}.[38] The FWHM is inversely proportional to the correlation length (grain size) of the domains, so these results suggest that the local spatial correlations between the domains were fixed during cross-linking.[38,39] In effect, the cross-linked nature of the P(S-*s*-GMA) domains prevented phase mixing across the domain interface and effectively trapped the domain composition inherent to the cross-linking temperature. The combination of the temperature dependence of $I(q^*)^{-1}$ and FWHM suggests that as the temperature was increased, thermal fluctuations and chain dynamics became increasingly important, and the domains began to "fluctuate", resulting in the observed increase in $I(q^*)^{-1}$. However, the cross-linked nature of the P(S-*s*-GMA) domain hindered mass exchange across the PLA and P(S-*s*-GMA) domain interface and fixed the correlation length, resulting in the observed temperature invariance of FWHM.

The sample that was cross-linked in the disordered state at 190 °C displayed a broad scattering peak at room temperature, characteristic of a disordered morphology. The temperature dependence of $I(q^*)^{-1}$ and FWHM for this sample was qualitatively similar to the sample cross-linked at 155 °C. The intensity of the principal scattering peak decreased with increasing temperature with a large upturn in $I(q^*)^{-1}$ observed above approximately 170 °C. Furthermore, the FWHM remained relatively constant across all of the measured temperatures. The initial disordered morphology was recoverable upon cooling the sample to 30 °C, suggesting that these observations represented a morphological change rather than sample degradation. As discussed for the sample cured at 155 °C, we believe that these results reflected domains whose relative spatial correlations were fixed by cross-linking yet still had sufficient mobility to rearrange with increasing temperature. Similar experiments were performed, and qualitatively similar results were obtained for P(S-*s*-GMA)-14-PLA-18-XGMA-29 + 0.3 wt % BTPH cured in the ordered state at 150 °C (T_{ODT} − 10 °C) and in the disordered state at 180 °C (T_{ODT} + 20 °C), Figure S22.

The ability of these cross-linked domains to rearrange with temperature was further investigated by heating cross-linked samples above their initial T_{ODT} and rapidly quenching them in liquid nitrogen to kinetically trap the morphology by vitrification.[35,40] A sample of P(S-*s*-GMA)-17-PLA-23-XGMA-27 + 0.3 wt % BTPH was first cured in the ordered state at 155 °C (T_{ODT} − 15 °C) and then heated above the T_{ODT} to 190 °C. After annealing the sample at this temperature for 1 h, it was removed from the oven and immediately quenched below T_g to kinetically trap the morphology present at 190 °C. The PLA domains were then selectively removed to facilitate SEM and N_2 sorption characterization of the domain structure and continuity (Figure 10).

The sample that was cured at 155 °C without subsequently heating above T_{ODT} displayed the expected lamellar morphology by SEM and low porosity by N_2 sorption analysis, consistent with an ordered morphology and minimal domain interconnectivity. In contrast, the sample that was cured at 155 °C and then quenched from 190 °C displayed a disordered morphology and a high porosity, suggesting that an ODT had occurred upon heating. The observed morphological changes support the conclusion that the cross-linked domains of P(S-*s*-GMA)-17-PLA-23-XGMA-27 retained a sufficiently high mobility to reorganize upon heating above T_{ODT}, which was consistent with the variable-temperature SAXS results. These results generally support the prevailing theoretical understanding that the ODT is primarily characterized by a change in interfacial curvature rather than by a significant change in domain composition,[8,36,41] as the cross-linked nature of these domains is expected to significantly hinder mass exchange and domain mixing. Samples that were cured in the disordered state at 190 °C displayed similarly disordered morphologies and high porosities regardless of whether they were examined in the as-cured state or were reheated and quenched from above T_{ODT}.

Interestingly, samples of P(S-*s*-GMA)-14-PLA-18-XGMA-29 + 0.3 wt % BTPH cured in the ordered state at 150 °C (T_{ODT} − 10 °C) did not display any morphological transition upon reheating and quenching from above T_{ODT} at 185 °C (Figure S23). Lamellar-like morphologies were observed for both the as-cured and the quenched samples after PLA removal. Furthermore, both samples displayed significantly lower porosities than a sample cured in the disordered state at 185 °C. One possible explanation for this lack of an observable morphological change may be related to the higher cross-link density for P(S-*s*-GMA)-14-PLA-18-XGMA-29 as compared to P(S-*s*-GMA)-17-PLA-23-XGMA-27. This is expected to reduce the chain mobility in the cross-linked domains and prevent their reorganization upon heating. Indeed, such a transition from a thermally accessible T_{ODT} to a permanently fixed and temperature invariant morphology has previously been reported for cross-linked block polymers with increasing cross-link density.[38,39] These observations are also consistent with the inability to orient the domains of P(S-*s*-GMA)-14-PLA-28-XGMA-29 postcuring in contrast to P(S-*s*-GMA)-17-PLA-23-XGMA-27, as their higher cross-link density may preclude them from aligning along the shear direction.

https://dx.doi.org/10.1021/acs.macromol.0c01424
Macromolecules 2020, 53, 7691−7704

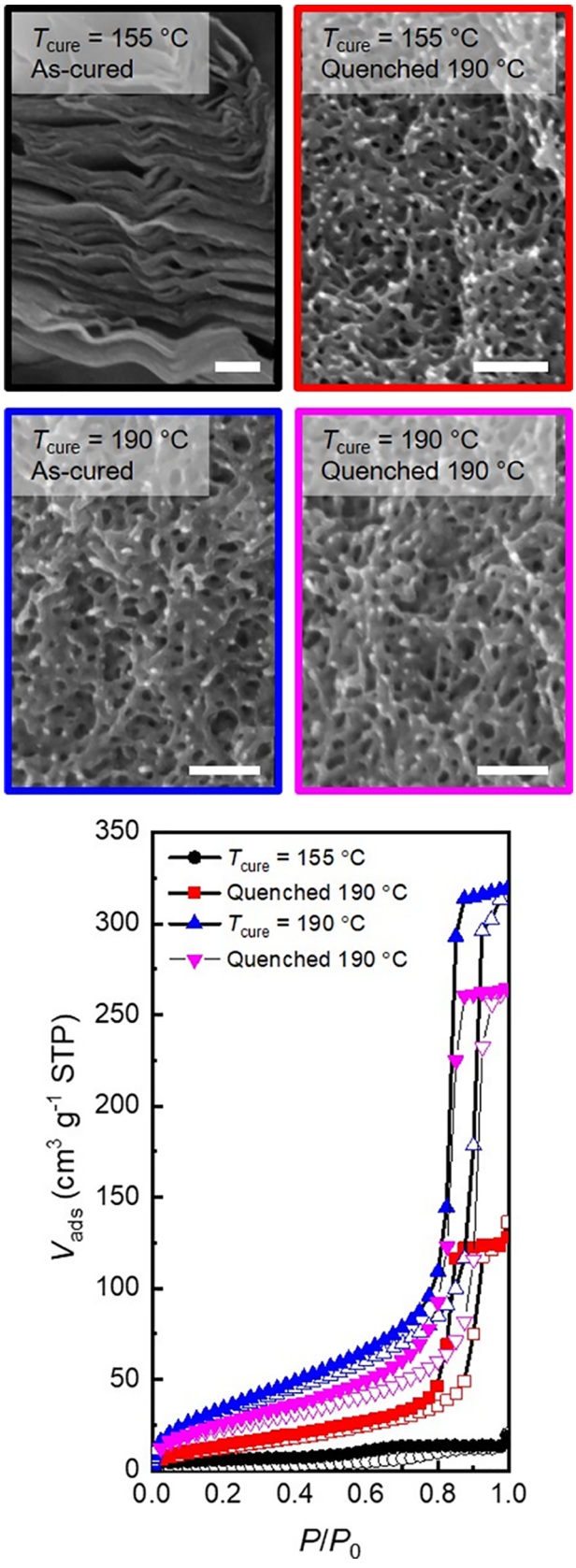

Figure 10. SEM images for P(S-*s*-GMA)-17-PLA-23-XGMA-27 + 0.3 wt % BTPH cured in the ordered state at 155 (T_{ODT} − 15 °C, top images) and the disordered state at 190 °C (T_{ODT} + 20 °C, bottom images). Following the initial curing, a section of each thermoset was then annealed above the T_{ODT} at 190 °C before rapidly quenching in liquid nitrogen. The SEM images of the as-cured monoliths (left images) and the quenched monoliths (right images) were obtained following PLA removal. All SEM samples were coated with approximately 2 nm of Ir and imaged at 3.0 kV. Nitrogen sorption isotherms for all etched monoliths (T_{cure} = 155 and 190 °C, the as-cured and quenched) are presented in the bottom panel.

However, these observations are not expected to significantly factor into the formation of kink bands. A more systematic investigation of these details may inform the design of novel adaptable materials from cross-linked block polymers.

CONCLUSIONS

LAOS was used to control the domain orientation for P(S-*s*-GMA)-*b*-PLA block polymers cross-linked in the disordered state. By varying the strain amplitude, the nanostructure of the disordered domains was precisely tuned during the simultaneous cross-linking reaction. For a given curing temperature slightly above T_{ODT}, a shear-induced DOT was observed with increasing strain amplitude because of the suppression of composition fluctuations. Rather than uniaxially aligned domains along the shear direction, parallel−transverse kinked lamellae were observed because of the large mechanical contrast between the domains. The effect of cross-linking temperature on this shear-induced DOT was then investigated by selecting several cross-linking temperatures both above and below T_{ODT} at a constant strain amplitude. For cross-linking temperatures near the T_{ODT} (both below and above), domain orientation and the formation of parallel−transverse kinked lamellae were observed under LAOS. However, there was no observable shear-induced DOT or domain alignment for cross-linking temperatures *far* above T_{ODT}. These results suggest that large amplitude composition fluctuations and/or slow curing kinetics relative to sample heating are required to obtain this transition. This point was further examined by first cross-linking samples under low strain amplitude and then applying LAOS post-gelation. For low cross-link densities, shear-induced domain orientation was observed parallel to the direction of shear, but the parallel−transverse orientation of samples cross-linked under LAOS was not observed. For a block polymer with a higher cross-link density, no alignment was observed post-gelation, presumably because of hindered chain mobility. These conclusions were supported by SAXS and SEM experiments for samples cross-linked in the ordered state and subsequently vitrified from above T_{ODT}. An ODT was observed for a diblock polymer with a low cross-link density while no such transition was observed for a diblock with a higher cross-link density. These findings demonstrate that the application of LAOS during the in situ cross-linking of a lamellar diblock polymer in the vicinity of the T_{ODT} can be a powerful tool to precisely control the alignment of microphase separated domains. Through the judicious selection of the cross-linking temperature and the strain amplitude, we have shown that it is possible to induce morphological transitions and to engineer the continuity and anisotropy of both the ordered and disordered states through mechanical processing.

ASSOCIATED CONTENT

Supporting Information

The Supporting Information is available free of charge at https://pubs.acs.org/doi/10.1021/acs.macromol.0c01424.

https://dx.doi.org/10.1021/acs.macromol.0c01424
Macromolecules 2020, 53, 7691−7704

Description of the synthesis of the P(S-*s*-GMA)-*b*-PLA block polymers; NMR spectra; size exclusion chromatography elugrams; DMA data (isothermal time sweeps for samples with and without BTPH); variable-temperature SAXS for uncross-linked and cross-linked samples; room-temperature SAXS patterns for cross-linked samples; SEM images for cross-linked samples; and N_2 sorption analysis for cross-linked samples (PDF)

AUTHOR INFORMATION

Corresponding Author

Marc A. Hillmyer − *Department of Chemistry, University of Minnesota, Minneapolis, Minnesota 55455, United States;* orcid.org/0000-0001-8255-3853; Email: hillmyer@umn.edu

Author

Nicholas Hampu − *Department of Chemical Engineering and Materials Science, University of Minnesota, Minneapolis, Minnesota 55455, United States;* orcid.org/0000-0002-8127-1034

Complete contact information is available at: https://pubs.acs.org/10.1021/acs.macromol.0c01424

Notes

The authors declare no competing financial interest.

ACKNOWLEDGMENTS

The authors thank Aaron Lindsay and Daphne Chan for the collection of some of the SAXS data, and Prof. Michelle Calabrese for carefully reading the manuscript. Altasorb generously donated lactide. Funding for this work was provided by the National Science Foundation (DMR-1609459 and DMR-2003454). Hitachi SU8320 SEM was provided by NSF MRI DMR1229263. Parts of this work were carried out in the Characterization Facility, UMN, which receives partial support from NSF through the MRSEC program. Portions of this work were performed at the DuPont-Northwestern-Dow Collaborative Access Team (DND-CAT) located at Sector 5 of the Advanced Photon Source (APS). DND-CAT is supported by Northwestern University, E. I. DuPont de Nemours & Co., and The Dow Chemical Company. This research used resources of the APS, a U.S. Department of Energy (DOE) Office of Science User Facility operated for the DOE Office of Science by Argonne National Laboratory under contract no. DE-AC02-06CH11357. Data were collected using an instrument funded by the NSF under award number 0960140.

REFERENCES

(1) Wang, D.; Kou, R.; Choi, D.; Yang, Z.; Nie, Z.; Li, J.; Saraf, L. V.; Hu, D.; Zhang, J.; Graff, G. L.; Liu, J.; Pope, M. A.; Aksay, I. A. Ternary Self-Assembly of Ordered Metal Oxide−Graphene Nanocomposites for Electrochemical Energy Storage. *ACS Nano* **2010**, *4*, 1587−1595.

(2) Werber, J. R.; Osuji, C. O.; Elimelech, M. Materials for next-Generation Desalination and Water Purification Membranes. *Nat. Rev. Mater.* **2016**, *1*, 16018.

(3) Peer, D.; Karp, J. M.; Hong, S.; Farokhzad, O. C.; Margalit, R.; Langer, R. Nanocarriers as an Emerging Platform for Cancer Therapy. *Nat. Nanotechnol.* **2007**, *2*, 751−760.

(4) Bates, F. S.; Fredrickson, G. H. Block Copolymers - Designer Soft Materials. *Phys. Today* **1999**, *52*, 32−38.

(5) Bates, F. S.; Fredrickson, G. H. Block Copolymer Thermodynamics: Theory and Experiments. *Annu. Rev. Phys. Chem.* **1990**, *41*, 525−557.

(6) Bates, C. M.; Bates, F. S. 50th Anniversary Perspective: Block Polymers—Pure Potential. *Macromolecules* **2017**, *50*, 3−22.

(7) Rosedale, J. H.; Bates, F. S.; Almdal, K.; Mortensen, K.; Wignall, G. D. Order and Disorder in Symmetric Diblock Copolymer Melts. *Macromolecules* **1995**, *28*, 1429−1443.

(8) Lee, S.; Gillard, T. M.; Bates, F. S. Fluctuations, Order, and Disorder in Short Diblock Copolymers. *AIChE J.* **2013**, *59*, 3502−3513.

(9) Bates, F. S.; Rosedale, J. H.; Fredrickson, G. H. Fluctuation Effects in a Symmetric Diblock Copolymer near the Order−disorder Transition. *J. Chem. Phys.* **1990**, *92*, 6255−6270.

(10) Bates, F. S.; Rosedale, J. H.; Fredrickson, G. H.; Glinka, C. J. Fluctuation-Induced First-Order Transition of an Isotropic System to a Periodic State. *Phys. Rev. Lett.* **1988**, *61*, 2229−2232.

(11) Sinturel, C.; Vayer, M.; Morris, M.; Hillmyer, M. A. Solvent Vapor Annealing of Block Polymer Thin Films. *Macromolecules* **2013**, *46*, 5399−5415.

(12) Feng, X.; Kawabata, K.; Cowan, M. G.; Dwulet, G. E.; Toth, K.; Sixdenier, L.; Haji-Akbari, A.; Noble, R. D.; Elimelech, M.; Gin, D. L.; Osuji, C. O. Single Crystal Texture by Directed Molecular Self-Assembly along Dual Axes. *Nat. Mater.* **2019**, *18*, 1235−1243.

(13) Mansky, P.; DeRouchey, J.; Russell, T. P.; Mays, J.; Pitsikalis, M.; Morkved, T.; Jaeger, H. Large-Area Domain Alignment in Block Copolymer Thin Films Using Electric Fields. *Macromolecules* **1998**, *31*, 4399−4401.

(14) Hadziioannou, G.; Mathis, A.; Skoulios, A. Obtention de ≪ Monocristaux ≫ de Copolymères Triséquencés Styrène/isoprène/styrène Par Cisaillement Plan. *Colloid Polym. Sci.* **1979**, *257*, 136−139.

(15) Cohen, Y.; Albalak, R. J.; Dair, B. J.; Capel, M. S.; Thomas, E. L. Deformation of Oriented Lamellar Block Copolymer Films. *Macromolecules* **2000**, *33*, 6502−6516.

(16) Koppi, K. A.; Tirrell, M.; Bates, F. S. Shear-Induced Isotropic-to-Lamellar Transition. *Phys. Rev. Lett.* **1993**, *70*, 1449−1452.

(17) Bates, F. S.; Koppi, K. A.; Tirrell, M.; Almdal, K.; Mortensen, K. Influence of Shear on the Hexagonal-to-Disorder Transition in a Diblock Copolymer Melt. *Macromolecules* **1994**, *27*, 5934−5936.

(18) Okamoto, S.; Saijo, K.; Hashimoto, T. Real-Time SAXS Observations of Lamella-Forming Block Copolymers under Large Oscillatory Shear Deformation. *Macromolecules* **1994**, *27*, 5547−5555.

(19) Pinheiro, B. S.; Hajduk, D. A.; Gruner, S. M.; Winey, K. I. Shear-Stabilized Bi-Axial Texture and Lamellar Contraction in Both Diblock Copolymer and Diblock Copolymer/Homopolymer Blends. *Macromolecules* **1996**, *29*, 1482−1489.

(20) Zeng, D.; Ribbe, A.; Kim, H.; Hayward, R. C. Stress-Induced Orientation of Cocontinuous Nanostructures within Randomly End-Linked Copolymer Networks. *ACS Macro Lett.* **2018**, *7*, 828−833.

(21) Panyukov, S.; Rubinstein, M. Stress-Induced Ordering in Microphase-Separated Multicomponent Networks. *Macromolecules* **1996**, *29*, 8220−8230.

(22) Aida, S.; Sakurai, S.; Nomura, S. Strain-Induced Ordering of Microdomain Structures in Polystyrene-Block-Polybutadiene-Block-Polystyrene Triblock Copolymers Cross-Linked in the Disordered State. *Polymer* **2002**, *43*, 2881−2887.

(23) Hampu, N.; Hillmyer, M. A. Temporally Controlled Curing of Block Polymers in the Disordered State Using Thermally Stable Photoacid Generators for the Preparation of Nanoporous Membranes. *ACS Appl. Polym. Mater.* **2019**, *1*, 1148−1154.

(24) Vidil, T.; Hampu, N.; Hillmyer, M. A. Nanoporous Thermosets with Percolating Pores from Block Polymers Chemically Fixed above the Order−Disorder Transition. *ACS Cent. Sci.* **2017**, *3*, 1114−1120.

(25) Hampu, N.; Bates, M. W.; Vidil, T.; Hillmyer, M. A. Bicontinuous Porous Nanomaterials from Block Polymers Radically Cured in the Disordered State for Size-Selective Membrane Applications. *ACS Appl. Nano Mater.* **2019**, *2*, 4567−4577.

(26) Hampu, N.; Hillmyer, M. A. Molecular Engineering of Nanostructures in Disordered Block Polymers. *ACS Macro Lett.* **2020**, *9*, 382−388.
(27) Kim, O.; Kim, S. Y.; Lee, J.; Park, M. J. Building Less Tortuous Ion-Conduction Pathways Using Block Copolymer Electrolytes with a Well-Defined Cubic Symmetry. *Chem. Mater.* **2016**, *28*, 318−325.
(28) Cates, M. E.; Milner, S. T. Role of Shear in the Isotropic-to-Lamellar Transition. *Phys. Rev. Lett.* **1989**, *62*, 1856−1859.
(29) Hamley, I. W. Structure and Flow Behaviour of Block Copolymers. *J. Phys.: Condens. Matter* **2001**, *13*, R643−R671.
(30) Stangler, S.; Abetz, V. Orientation Behavior of AB and ABC Block Copolymers under Large Amplitude Oscillatory Shear Flow. *Rheol. Acta* **2003**, *42*, 569−577.
(31) Bertrand, A.; Hillmyer, M. A. Nanoporous Poly(lactide) by Olefin Metathesis Degradation. *J. Am. Chem. Soc.* **2013**, *135*, 10918−10921.
(32) Polis, D. L.; Winey, K. I. Kink Bands in a Lamellar Diblock Copolymer Induced by Large Amplitude Oscillatory Shear. *Macromolecules* **1996**, *29*, 8180−8187.
(33) Polis, D. L.; Winey, K. I. Controlling Kink Band Morphology in Block Copolymers: Threshold Criteria and Stability. *Macromolecules* **1998**, *31*, 3617−3625.
(34) Zeng, D.; Ribbe, A.; Hayward, R. C. Anisotropic and Interconnected Nanoporous Materials from Randomly End-Linked Copolymer Networks. *Macromolecules* **2017**, *50*, 4668−4676.
(35) Hampu, N.; Hillmyer, M. A. Molecular Engineering of Nanostructures in Disordered Block Polymers. *ACS Macro Lett.* **2020**, *9*, 382−388.
(36) Medapuram, P.; Glaser, J.; Morse, D. C. Universal Phenomenology of Symmetric Diblock Copolymers near the Order−Disorder Transition. *Macromolecules* **2015**, *48*, 819−839.
(37) Gillard, T. M.; Phelan, D.; Leighton, C.; Bates, F. S. Determination of the Lamellae-to-Disorder Heat of Transition in a Short Diblock Copolymer by Relaxation Calorimetry. *Macromolecules* **2015**, *48*, 4733−4741.
(38) Gomez, E. D.; Das, J.; Chakraborty, A. K.; Pople, J. A.; Balsara, N. P. Effect of Cross-Linking on the Thermodynamics of Lamellar Block Copolymers. *Macromolecules* **2006**, *39*, 4848−4859.
(39) Hahn, H.; Chakraborty, A. K.; Das, J.; Pople, J. A.; Balsara, N. P. Order-Disorder Transitions in Cross-Linked Block Copolymer Solids. *Macromolecules* **2005**, *38*, 1277−1285.
(40) Hickey, R. J.; Gillard, T. M.; Irwin, M. T.; Lodge, T. P.; Bates, F. S. Structure, Viscoelasticity, and Interfacial Dynamics of a Model Polymeric Bicontinuous Microemulsion. *Soft Matter* **2016**, *12*, 53−66.
(41) Yadav, M.; Bates, F. S.; Morse, D. C. Network Model of the Disordered Phase in Symmetric Diblock Copolymer Melts. *Phys. Rev. Lett.* **2018**, *121*, 127802.

https://dx.doi.org/10.1021/acs.macromol.0c01424
Macromolecules 2020, 53, 7691−7704